Optical phonons in $SnGeS_3$

Zoran V. Popović
Institute of Physics, P.O. Box 57, 11001 Beograd, Yugoslavia
(Received 28 November 1984)

The polarized infrared and Raman spectra of $SnGeS_3$ are reported. Infrared-active phonon frequencies and dielectric constants are obtained by oscillator fitting of reflectivity data. A group-theoretical analysis of the crystal, one of its constituent layers, and the $(GeS_2S^{2-}_{2/2})_\infty$ chain has been performed to identify the symmetries of the observed modes. A force-constant anisotropy of about 50 between the intralayer and interlayer forces is deduced from rigid-layer mode and Davydov splitting observations.

I. INTRODUCTION

Tin germanium trisulfide belongs to the ternary-sulfide group of the $A^{II}B^{IV}S_3$ configuration where A^{II} may be Sn or Pb and B^{IV} is either Ge or Sn. The properties of these semiconductors are still not well known. Ternary sulfides are obtained from binary sulfides in reactions involving the respective binary-sulfide constituent elements. These compounds comprise two isomorphic groups with orthorhombic ($A^{II}SnS_3$) and monoclinic ($A^{II}GeS_3$) crystal structure.

The structure of these compounds has been the topic of many papers.[1–4] Their crystal growth and certain optical and transport properties have been dealt with.[5] The infrared and Raman spectra of $Sn^{II}Sn^{IV}S_3$ have also been reported in Ref. 6. Preliminary $PbGeS_3$ and $SnGeS_3$ vibrational spectra were discussed in our earlier papers.[7,8]

The $SnGeS_3$ was obtained by the thermal annealing of a SnS and GeS_2 solution at 500 °C. The $SnGeS_3$ melting point is at 609 °C, it has an energy gap of $E_g = 2.23$ eV and an electrical conductivity of the order of 10^{-8} $(\Omega\,\mathrm{m})^{-1}$. The compound is of interest because $SnGeS_3$ is a photoconductor with a spectral sensitivity peak at 500 nm[5]. The unit-cell parameters of $SnGeS_3$ are given in Table I.

The $SnGeS_3$ crystal structure shown in Fig. 1 is given in terms of coordination tetrahedra in the *bc* and *ab* planes. The basic building blocks of the $SnGeS_3$ structure are corner-sharing GeS_4 tetrahedra that form $(GeS_2S^{2-}_{2/2})_\infty$ chains along the *c* axis. The $SnGeS_3$ unit cell consists of two of these chains of two tetrahedra each that are linked via the Sn atoms. Each Sn atom is surrounded by five S atoms, forming a deformed SnS_5 quadratic pyramid. The two layers comprising the $SnGeS_3$ unit cell are parallel to the *bc* plane and normal to the *a* axis of the crystal. The average spacing between the Ge and S atoms within GeS_4 tetrahedra is 0.223 nm, the average spacing between the Sn and S atoms ranging from 0.263 nm and 0.2937 nm (mean value 0.2859 nm).

In this paper, the vibrational properties of $SnGeS_3$ were investigated using far-infrared and Raman spectroscopy and analyzed on the basis of specifics of the $SnGeS_3$ crystal structure. The observed modes were identified by crystal, layer, and chain factor-group analysis (FGA). The experimental details and results are presented in Sec. II. The factor-group analyses and oscillator fittings of the measured ir reflectivity spectra are given in Sec. III. Finally, in Sec. IV, the one-dimensional, two-dimensional, and three-dimensional approaches are used to discuss the vibrational properties of $SnGeS_3$.

II. EXPERIMENT

The $SnGeS_3$ crystals we used were obtained by the gas-transport technique. A detailed description of this process was given in an earlier paper.[5] Freshly cleaved samples were used to measure reflectivity spectra. The far-infrared measurements were obtained at room temperature using a Brucker IFS 114 spectrometer with polarized light in the (20—500)-cm^{-1} range.

TABLE I. Crystallographic parameters of $SnGeS_3$.

Unit-cell parameters	
Z	4
a (nm)	0.7269
b (nm)	1.022
c (nm)	0.6873
β (deg)	105.45
Crystal symmetry	monoclinic
Space group	$P_{2_1/c}$

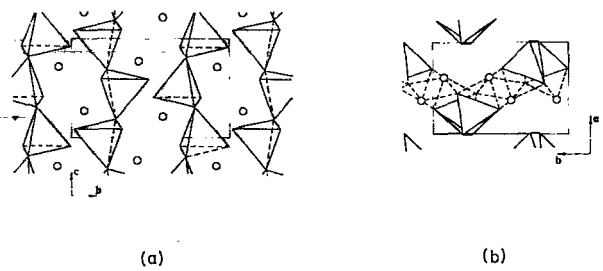

FIG. 1. Crystal structure of $SnGeS_3$ shown in terms of the coordination tetrahedra in the (a) *bc* plane and (b) *ab* plane.

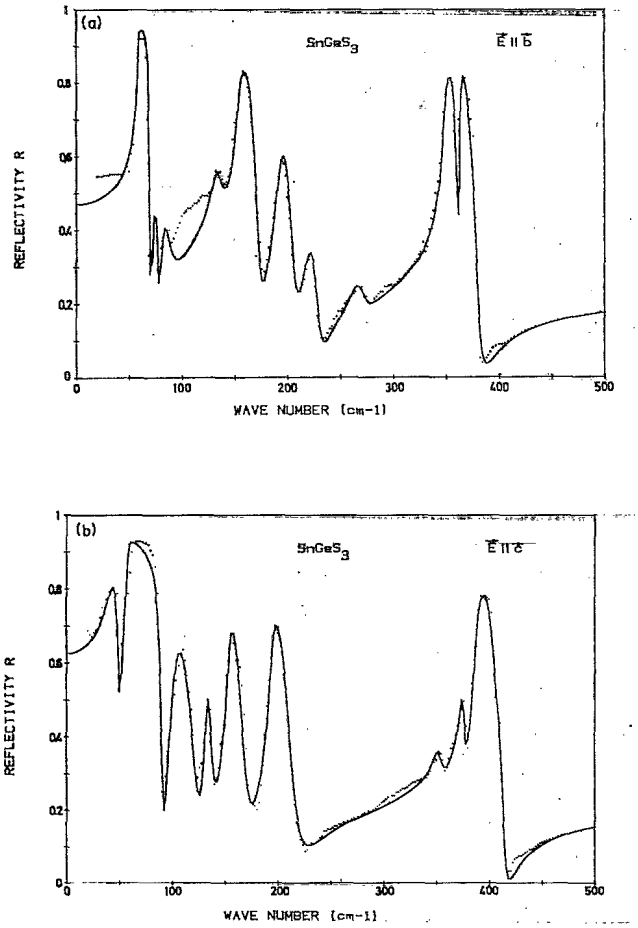

FIG. 2. Room-temperature far-infrared reflectivity spectra of $SnGeS_3$ for (a) $\mathbf{E}||\mathbf{b}$ and (b) $\mathbf{E}||\mathbf{c}$ polarization.

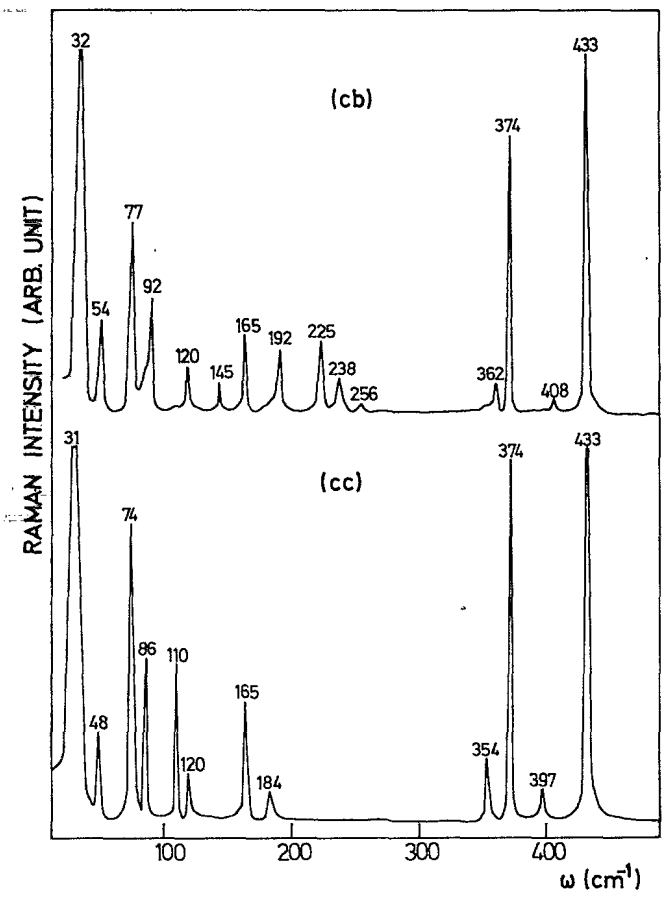

FIG. 3. Raman spectra of $SnGeS_3$ at liquid-helium temperature.

Raman spectra were observed in the backscattering geometry at 4.2 K. Spex and Jarrel-Ash monochromators equipped with holographic gratings were used. A RCA model No. 31034A photomultiplier we used was Peltier-effect cooled down to -20°C. The excitation sources were the 514.5 and 501.7 nm lines of an Ar^+ Spectra Physics ion laser.

The polarized $SnGeS_3$ reflectivity spectra for $\mathbf{E}||\mathbf{b}$ and $\mathbf{E}||\mathbf{c}$ polarizations at 300 K are shown in Fig. 2. The spectra were obtained with a resolution of 2 cm^{-1}. The points are experimental values whereas the solid curves were obtained on the basis of a model to be presented in Sec. III B. In Figs. 2(a) and 2(b), ten oscillators can be observed for both the $\mathbf{E}||\mathbf{b}$ and $\mathbf{E}||\mathbf{c}$ polarizations, respectively.

The Raman spectra for (cb) and (cc) polarizations at 4.2 K are shown in Fig. 3. The (xy) denotes that the incident light is polarized parallel to the x crystal axis while the polarization of the scattered light is parallel to the y crystal axis. Fifteen modes can be identified for (cb), while 12 Raman-active modes can be identified for (cc). Thus 27 Raman-active modes and 20 infrared-active modes have been observed in all.

III. ANALYSIS

A. Factor-group analysis

The $SnGeS_3$ unit cell consists of 4 molecules comprising 20 atoms in all (Table I). Since all the atoms of the unit cell have C_1 site symmetry, the 60 vibrational modes of the $P_{2_1/c}$ space group decompose according to the following representation:

$$\Gamma^{\text{cryst}} = 15A_g + 15B_g + 15A_u + 15B_u \ , \tag{1}$$

where, of the above, $1A_u + 2B_u$ are acoustic modes. There are, thus 57 optically active modes. Thirty of them are Raman-active (g) and 27 are infrared-active (u) modes. The experimental conditions in which the optical modes of the $P_{2_1/c}$ space group were observed (Fig. 4) differ from the conditions referred to in the greater part of the literature.[9] Namely, in our case $C_2^y||\mathbf{b}$ (second setting) and the z and y coordinates change places in the C_{2h} point-group character table. The basic functions become

A_g: xx,yy,zz,xz ,

B_g: yz,xy ,

A_u: T_y ,

B_u: T_x,T_z .

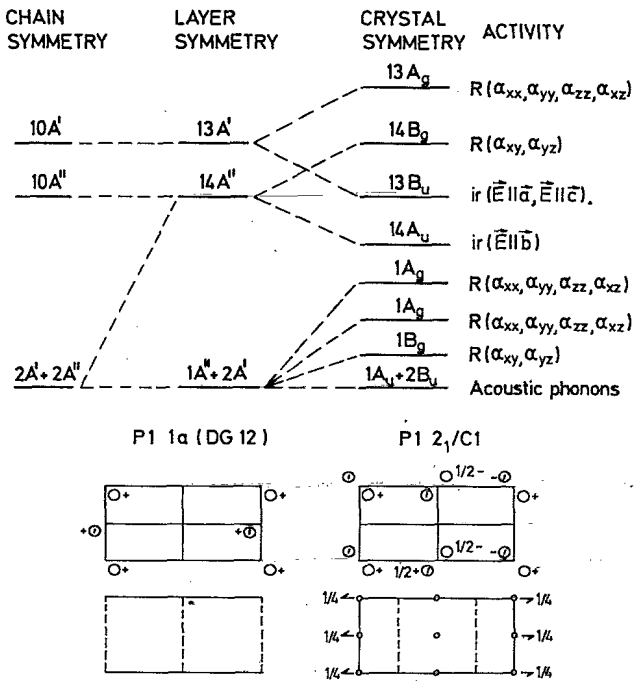

FIG. 4. Compatibility diagram relating the chain, layer, and crystal vibrations of $SnGeS_3$.

The $SnGeS_3$ *bc* cleavage plane is accordingly well suited for the determination of all the basic functions of the $P_{2_1/c}$ space group.

B. Oscillator fitting

Oscillator fitting of the reflectivity data was used to obtain the frequencies of the infrared-active modes. The theoretical curves, shown in Fig. 2, were obtained according to the factorized dielectric constant model

$$\epsilon=\epsilon_\infty \prod_{j=1}^{n} \frac{\omega_{jLO}^2-\omega^2-i\omega\gamma_{jLO}}{\omega_{jTO}^2-\omega^2-i\omega\gamma_{jTO}}, \tag{2}$$

where ω_{jTO} and γ_{jTO} are the transverse frequency and damping coefficients, ω_{jLO} and γ_{jLO} are the longitudinal frequency and damping coefficients, and ϵ_∞ is the dielectric constant at very high frequencies.

The solid curves in Fig. 2 are the spectra in accordance with the above model. Best oscillator fit parameters are listed in Table II. The static dielectric constant which is given in Table II is obtained using the generalized Lyddane-Sachs-Teller (LST) relation:

$$\epsilon_0=\epsilon_\infty \prod_{j=1}^{n} \frac{\omega_{jLO}^2}{\omega_{jTO}^2}. \tag{3}$$

IV. DISCUSSION

Factor-group analysis of $SnGeS_3$ yields $13A_u$ and $14B_u$ or a total of 27 infrared-active modes. Experimentally, only $10A_u$ and $10B_u$ have been observed. This is $3A_u$ and $4B_u$ modes short of the FGA predicted number. In order to account for the discrepancy between the FGA predicted and actually observed number of infrared active modes, the vibrational properties of one layer of $SnGeS_3$ atoms, and of the $(GeS_2S_{2/2}^{2-})_\infty$ chain are considered. The $SnGeS_3$ crystal is a layer crystal with interlayer bonds that are much weaker than the intralayer bonds. Thus, the vibrational properties of the crystal are predominantly due to the vibrational behavior of the layer. In considering the vibrational properties of the individual isolated layer, we break the periodicity in the direction perpendicular to the

TABLE II. Phonon frequencies (cm^{-1}) and dielectric constants obtained by oscillator fitting of the reflectivity spectra of $SnGeS_3$.

	ω_{TO}	γ_{TO}	ω_{LO}	γ_{LO}	ϵ_0	ϵ_∞
E||b	59	1	70	1.2		
	74	5.5	78	3		
	82	8	88	20		
	133	9	136	15		
	154	6	173	10	29	8
	192	10	206	12		
	220	14	230	12		
	268	14	271	17		
	349	4	361	3		
	363	2	381	9		
E||c	42	9	50	4		
	58	2	91	4		
	102	8	124	13		
	133	4	138	10		
	154	5	170	16		
	194	6	216	20	73	7.5
	352	10	354	12		
	374.5	5	377	5		
	387	7	406	12		
	408	13	414	5		

layer. Due to this, the layer optical vibrational activity is studied in terms of diperiodic groups[10,11] rather than triperiodic space groups.

The structure of the $SnGeS_3$ layer is shown in Fig. 5(a). As a $SnGeS_3$ layer consists of a $(GeS_2S^{2-}_{2/2})_\infty$ chain and Sn atoms, two layer-symmetry operations are required, an identity and a $\bar{c}$ glide plane. The $DG12$ (Ref. 10) diperiodic group is the only symmetry operation group of the 80 that has both an identity and a glide plane. This diperiodic group is isomorphic with the C_s point group. In this case of layer symmetry, the normal mode distribution is

$$\Gamma^{\text{layer}}=15A'+15'' , \tag{4}$$

where A' and A'' are both Raman- and ir-active modes. The compatibility diagram relating the layer and crystal vibration of $SnGeS_3$ is given in Fig. 4. The A' layer modes split into A_g-B_u doublets. The A'' layer modes decompose into B_g-A_u crystal symmetry doublets (Davydov splitting). Layer A' modes have been observed in the Raman spectra for $(xx),(yy),(zz),(xz)$ and in the ir spectra for E parallel to the ac plane. The conditions under which the A' modes observed differ from those encountered in the character tables for the C_s point group because in our case the $SnGeS_3$ layer symmetry is $\sigma_h \perp \mathbf{b}$. Layer factor-group analysis yields identical frequencies for the Raman and ir modes, while crystal FGA results in different frequencies for the Raman and ir lines. According to the compatibility diagram in Fig. 4, the closer the frequencies of the corresponding modes, the more pronounced is the layer structure. We shall later see that the difference in frequency between corresponding ir and Raman lines will give us the ratio of the intralayer to interlayer bond strengths.

The last three $(2A_g+B_g)$ Raman-active modes in Fig. 4 are acoustical branch layer modes. They are the so-called rigid-layer modes (RLM).[11] These rigid-layer modes are due to the vibration of the layers as very nearly rigid molecular units. Two shear modes and a compression mode can be identified.

The structure of a $SnGeS_3$ layer has already been discussed and is illustrated in Fig. 5(a). The layer consists of a $(GeS_2S^{2-}_{2/2})_\infty$ chain and Sn atoms. As the average Ge-S spacing of 0.223 nm is considerably smaller than the average S-Sn spacing of 0.2859 nm, it may be assumed that the effect of the Sn atoms on the vibrational properties of the layer is not significant. Thus the $(GeS_2S^{2-}_{2/2})_\infty$ chain behaves as an isolated molecular unit and we can compute its vibrational-mode optical activity. The structure of the $(GeS_2S^{2-}_{2/2})_\infty$ chain and its symmetry operations, and identity and $\bar{c}$ glide plane are given in Fig. 5(b). These operations belong to a second-order symmetry operation group that is isomorphic with the C_s point group. As can be seen in Fig. 5(b), the basic repeating unit of the chain consists of six S and two Ge atoms, eight atoms in all. These atoms have C_1 site symmetry and the following normal mode distribution:

$$\Gamma^{\text{chain}}_{\text{tot}}=12A'+12A'' . \tag{5}$$

The translational modes

$$\Gamma_{\text{trans}}=2A'+1A'' \tag{6}$$

and the rotational mode due to rotation around the c chain axis

$$\Gamma_{\text{rot}}=1A'' \tag{7}$$

have to be subtracted from (5) to obtain the optical-active-mode distribution of the $(GeS_2S^{2-}_{2/2})_\infty$ chain:

$$\Gamma^{\text{chain}}=10A'+10A'' , \tag{8}$$

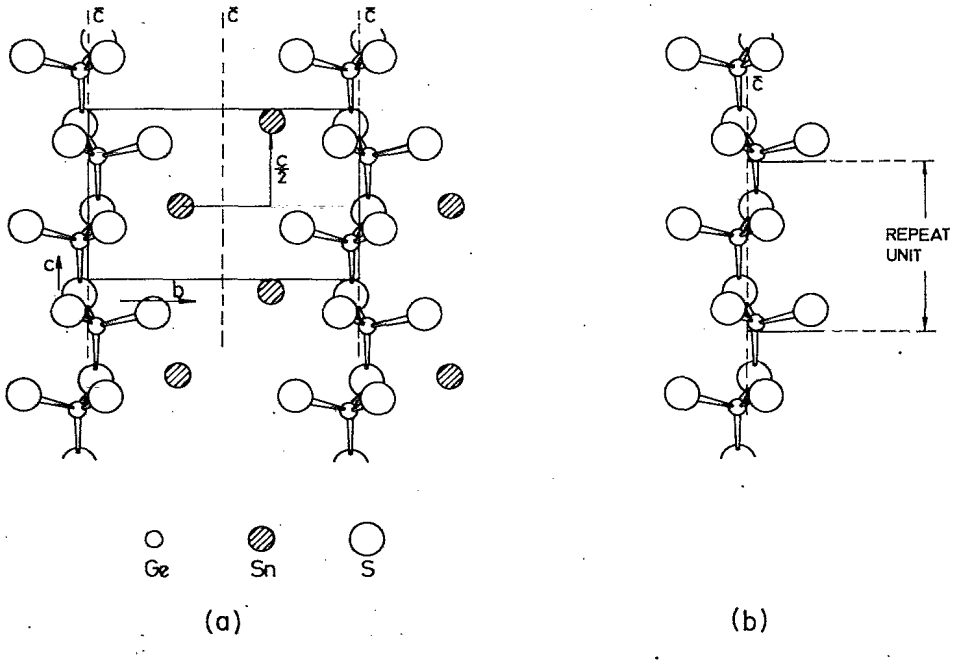

FIG. 5. (a) Structure of single layer of $SnGeS_3$ and (b) structure of the $(GeS_2S^{2-}_{2/2})_\infty$ chain with symmetry operations.

TABLE III. Frequencies (cm^{-1}) of some of the doublets of infrared- and Raman-active phonons together with the respective values of ν_0, Δ, and $(\nu_0/\Delta)^2$.

A_u-B_g					B_u-A_g				
ν_+	ν_-	ν_0	Δ	$(\nu_0/\Delta)^2$	ν_+	ν_-	ν_0	Δ	$(\nu_0/\Delta)^2$
59	54	56,5	17	11	42	48	45	16	8
74	77	75,5	15	25	58	74	66	33	4
82	92	87	29	9	102	110	106	29	13
133	120	127	41	10	133	120	127	41	10
154	145	150	37	17	154	165	160	42	15
192	192	192	0		194	184	189	43	19
220	225	222.5	33	45	352	354	353	27	176
268	256	262	56	22	374	374	374	0	
363	362	362.5	19	362	387	397	392	63	39

where A' chain modes are observed for $\mathbf{E}||$ the ac plane, i.e., (xx), (yy), (zz), and (xz), and A'' modes are observed for $\mathbf{E}||\mathbf{b}$, i.e., (xy) and (yz). These conditions coincide with the conditions for the observation of layer modes. The chain, layer, and $SnGeS_3$ crystal vibrational-mode compatibility diagram is given in Fig. 4.

Since $(GeS_2S^{2-}_{2/2})_\infty$ chain FGA actually predicts the observed number of $10A'$ ($\mathbf{E}||\mathbf{c}$) and $10A''$ ($\mathbf{E}||\mathbf{b}$) modes, $(GeS_2S^{2-}_{2/2})_\infty$ chain vibrations dominate the $SnGeS_3$ infrared spectra. This was to be expected, as the intrachain spacings are smaller and the bonding stronger than between S and Sn atoms and between S atoms belonging to different chains or layers.

The agreement between the observed reflectivity spectra and the spectra obtained from (2) for the $\mathbf{E}||\mathbf{c}$ polarization is exceptionally good. For the $\mathbf{E}||\mathbf{b}$ polarization, disagreement between computed and observed spectra occurs only in the (90—130)-cm^{-1} range. We are of the opinion that this due to leakage of the $\mathbf{E}||\mathbf{c}$ oscillator with $\omega_{TO}=102$ cm^{-1}. The only effect is the raising of the reflectivity spectrum within this range, the existence of a new oscillator not being clearly observed.

The FGA of $SnGeS_3$ crystal predicts 30 Raman-active modes. $12A_g$ and $15B_g$ modes are observed in the experimental spectra shown in Fig. 3. This is $3A_g$ modes less than the predicted number. As the number of observed Raman active modes exceeds the number of $(GeS_2S^{2-}_{2/2})_\infty$ chain modes, the Raman spectra consists of chain, layer, and unit-cell vibrational modes.

According to the compatibility diagram in Fig. 4, the A' chain or layer modes split into A_g-B_u crystal doublets. A comparison of the Raman spectra in Fig. 3 and the ir active modes tabulated in Table II yields both A_g-B_u and B_g-A_u doublets. These are given in Table III, where a (1—16)-cm^{-1} frequency difference between corresponding Raman (ν_-) and infrared (ν_+) modes can be observed. Table III also contains entries for ν_0, Δ, and $(\nu_0/\Delta)^2$ that are defined in terms of $\nu_\pm$ by the following simple relationship:[11]

$$\nu_\pm=(\nu_0^2\pm\Delta^2)^{1/2}, \tag{9}$$

valid for a pair of weakly coupled identical oscillators where ν_0 is the isolated-oscillator frequency and Δ^2 is proportional to the coupling force constant. The ratio of intralayer to interlayer bonding strengths is proportional to $(\nu_0/\Delta)^2$. The mean value of $(\nu_0/\Delta)^2$ in Table III is approximately 50, indicating that the bonds within a layer are 50 times stronger than interlayer bonds.

The values of Δ in Table III vary from 15 to 63, falling into the rigid-layer (RL) mode range. Namely, the last three lines in Fig. 4, $2A_g+1B_g$, are acoustic-branch layer symmetry modes and are only Raman active. These modes are due to the vibration of whole layers as molecular units in respect to each other. Two shear modes and a compression mode can be observed. The shear-mode frequencies being lower than the compression mode frequency. The $SnGeS_3$ RL modes were identified by a comparison of the Raman and infrared spectra in the (20—100)-cm^{-1} range. The (20—100)-cm^{-1} portion of the ir spectra is shown in Fig. 6(b). Upon comparison of these spectra with the Raman spectra given in Fig. 3, it becomes evident that the Raman modes at 31 and 86 cm^{-1} (A_g) and 32 cm^{-1} (B_g) do not have ir analogs. They are Raman active, only. It can thus be assumed that they are actually rigid-layer modes. The 31-cm^{-1} (A_g) and 32-cm^{-1} (B_g) lines are shear modes while the 86-cm^{-1} (A_g) line is a compression mode.

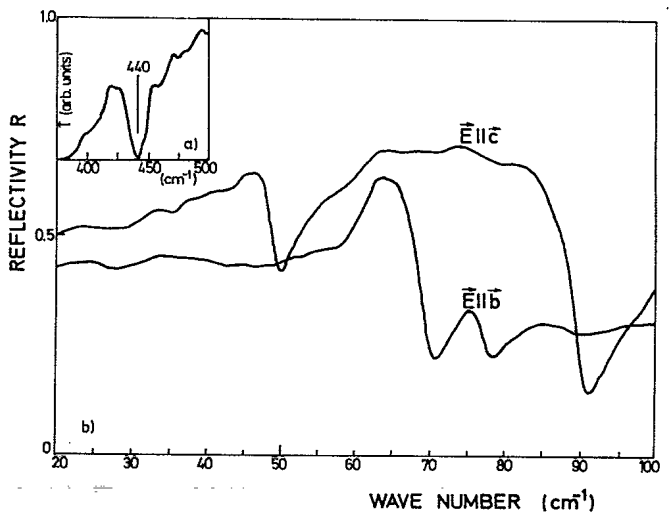

FIG. 6. ir spectra of $SnGeS_3$. (a) Nonpolarized transmission spectra in the range from 400 to 500 cm^{-1}. (b) Polarized reflection spectra in the range from 20 to 100 cm^{-1}.

We will now consider the strong Raman mode at 433 cm^{-1} in Fig. 3. No ir-active mode corresponding to the above Raman mode is observed in the reflection spectra in Fig. 2, although one is predicted by the compatibility diagram in Fig. 4. However, this Raman line at 433 cm^{-1} is not a laser plasma line. The laser line used was the 514.5-nm line of the Ar^+ laser. The 541.5-nm line has plasma lines at 267 and 521 cm^{-1}. Also, an interference filter was used in obtaining the Raman spectra.

Thus, we are of the opinion that there is a $SnGeS_3$ mode at 433 cm^{-1} and that the corresponding infrared mode is too weak to be detected in the reflection spectra.

The nonpolarized $SnGeS_3$ transmission spectra in Fig. 6(a) between 400 and 500 cm^{-1} also confirm the above conclusions. A $SnGeS_3$ ir-active mode at about 440 cm^{-1} can be observed. The remaining ir-active modes below 400 cm^{-1} could not be observed in the transmission spectra due to the strong absorption caused by the present oscillators below 400 cm^{-1}. Thus the spectra in this region contains no useful information.

The above was also observed for GeS_2, where the $(GeS_2S^{2-}_{2/2})_\infty$ chain is also the basic building block. The GeS_2 ir mode corresponding to the Raman mode at the highest frequency was observed only in the transmission spectra.[14]

Let us once again consider Figs. 2 and 3, in which the $SnGeS_3$ ir and Raman spectra, are shown, respectively. Two spectral regions on the diagrams are of interest, from 350 cm^{-1} to 450 cm^{-1} and below 300 cm^{-1}. The (350—450)-cm^{-1} region is due to the bond-stretching vibrations of corner-sharing GeS_4 tetrahedra. The region below 300 cm^{-1} is due to bond-bending GeS_4 tetrahedral vibrations. If the Ge—S bond is adopted as the internal coordinate, a FGA of the bond-stretching $(GeS_2S^{2-}_{2/2})_\infty$ chain vibrations can be performed. Namely, the repeat chain unit has eight Ge—S bonds [Fig. 5(b)] and has C_s point-group symmetry. Thus the bond-stretching vibrations decompose according to the following irreducible representation:

$$\Gamma^{BS}=4A'+4A'' . \tag{10}$$

The $4A'+4A''$ observed bond-stretching Raman modes in the spectra in Fig. 3 are in agreement with the predictions of (10). Four ir bond-stretching modes for the $\mathbf{E}||\mathbf{c}$ polarization (A') and two for $\mathbf{E}||\mathbf{b}$ polarization (A'') modes have been observed. Thus, of the predicted 8 Raman and ir bond-stretching modes, we have observed 8 Raman and 6 ir modes. This is in good agreement with the predictions.

A detailed analysis of the molecular vibrations in germanium dichalcogenides and trichalcogenides has been presented in our earlier papers.[12,13]

V. SUMMARY

The vibrational properties of $SnGeS_3$ were discussed in terms of the vibrational behavior of the $(GeS_2S^{2-}_{2/2})_\infty$ chain, one layer, and the whole crystal because the crystal is a layered structure with the $(GeS_2S^{2-}_{2/2})_\infty$ chain as the basic layer building block. FGA was performed for the chain, layer, and crystal. The presented polarized ir and Raman spectra, both in terms of shape and the number of present active ir modes confirm the dominant role played by chain vibrations. The existence of Raman-ir Davydov doublets as well as the appearance of $SnGeS_3$ rigid layer modes validates the layer symmetry assumption. The frequency difference of the Raman-infrared doublets yields an intralayer-to-interlayer bond strength ratio of about 50.

ACKNOWLEDGMENTS

The experiments discussed were performed at the Max-Planck Institut für Festkörperforschung in Stuttgart. I would like to thank J. Fenner for the $SnGeS_3$ single crystals used, W. Köning for help with the infrared experiment, and Dr. J. Stolz for helpful discussions. I am grateful for the hospitality of the Max-Planck-Institut and I am indebted to Professor Dr. M. Cardona for his kindness during my stay.

[1]D. Mootz and H. Puhl, Acta Crystallogr. **23**, 471 (1967).
[2]J. C. Jumas, M. Ribes, E. Philippot, and M. Maurin, C. R. Acad. Sci. Ser. C **275**, 269 (1972).
[3]J. Fenner and D. Mootz, Z. Anorg. Allg. Chem. **427**, 123 (1976).
[4]M. Ribes, J. Olivier-Fourcade, E. Philippot, and M. Maurin, Acta Crystallogr. Sect. B **30**, 1391 (1974).
[5]U. V. Alpen, J. Fenner, and E. Gmelin, Mater. Res. Bull. **10**, 175 (1975).
[6]H. R. Chandrasekhar and D. G. Mead, Phys. Rev. B **19**, 932 (1979).
[7]Z. V. Popović, Physica **119B**, 283 (1983).
[8]Z. V. Popović and H. J. Stolz, Fizika **14**, 35 (1982).
[9]E. B. Wilson, J. C. Decius, and P. C. Cross, *Molecular Vibrations* (McGraw-Hill, New York, 1955).
[10]E. A. Wood, The 80 Diperiodic Groups in Three Dimensions, Bell Telephone System Technical Monograph No. 4680, 1964 (unpublished).
[11]R. Zallen, M. L. Slade, and A. T. Ward, Phys. Rev. B **3**, 4257 (1971).
[12]Z. V. Popović, Phys. Lett. **94A**, 242 (1983).
[13]Z. V. Popović, Fizika **15**, 11 (1983).
[14]Z. V. Popović and H. J. Stolz, Phys. Status Solidi B **106**, 337 (1981).